Geophys. J. Int. (2003) **155,** 33–43

Time-domain, spectral finite-element approach to transient 2-D geomagnetic induction in a spherical heterogeneous Earth

Zdeněk Martinec,[1,*] Mark E. Everett[2] and Jakub Velímský[3]

[1] *GeoForschungsZentrum Potsdam, Division* 1: *Kinematics and Dynamics of the Earth, Telegrafenberg,* D-14473, *Potsdam, Germany*
[2] *Department of Geology and Geophysics, Texas A&M University, College Station,* TX 77843, *USA*
[3] *Department of Geophysics, Faculty of Mathematics and Physics, Charles University, V Holešovičkách* 2, 18000 *Prague* 8, *Czech Republic*

Accepted 2003 February 25. Received 2002 June 17; in original form 2001 November 8

SUMMARY

A time-domain, spectral finite-element approach is presented for computing the electromagnetic induction response of a 2-D heterogeneous conducting sphere to transient external current excitation. This method is appropriate for determining the induced spatiotemporal electromagnetic signature at satellite altitudes associated with the upper and mid-mantle conductivity heterogeneities. The new approach is based on an existing frequency-domain 2-D spectral finite-element technique modified by the implementation of a time-stepping algorithm. To validate the time-domain approach and the associated numerical code, transient responses of concentrically and eccentrically nested spheres to ring-current excitations are computed using the inverse Fourier transform of analytical and semi-analytical, frequency-domain solutions. We show that the time-domain approach is particularly appropriate when the external current excitation has a transient feature. Compared with the frequency-domain method, it may significantly reduce the computation time while maintaining the time resolution.

Key words: electrical conductivity, electromagnetic induction, explicit time differencing, linear finite elements, spherical harmonics.

1 INTRODUCTION

Electrical conductivity is an important deep-Earth physical property, the spatial variations of which contain fundamental information concerning geodynamic processes such as the subduction of slabs, the ascent of mantle plumes and the convection of anomalously hot mantle material. The electrical conductivity of the upper to mid mantle is conventionally studied using frequency-domain geomagnetic induction techniques. The traditional approach involves the estimation of surface impedances from land-based observatory recordings of geomagnetic time variations in the period range of several hours to several days. The underlying electrical conductivity is extracted from the measured impedances by means of forward modelling and inversion. The task is difficult, however, since the observatory network is sparse and irregularly distributed over the globe, while the time-series themselves are intermittent and of highly variable quality.

At the present time, there exists an unprecedented opportunity to use satellite magnetometer records to improve our knowledge of global electrical conductivity. The recently launched Oersted (1999 February) and CHAMP (2000 July) satellites are returning high-precision vector and scalar measurements of the geomagnetic field from low-Earth orbits. A magnetic satellite such as Oersted (e.g. Neubert *et al.* 2001) samples both the spatial and the temporal variations associated with fluctuating magnetospheric, ionospheric and internal current systems. Unlike land-based observatories, satellites acquire data with no regard for oceans and continents, hemispheres or political boundaries. Satellite induction data are more difficult to analyse than their terrestrial counterparts, which show only temporal variations.

To quantitatively model 3-D induction effects in the geomagnetic field at satellite altitudes, a transient 3-D electromagnetic induction in a heterogeneous sphere needs to be simulated. Several techniques are available to model the geomagnetic response of a 3-D heterogeneous sphere in the Fourier-frequency domain, each based on a different numerical method: spherical thin-sheet analysis (Fainberg & Singer 1980; Kuvshinov *et al.* 1999a), finite-element analysis (Everett & Schultz 1996; Weiss & Everett 1998), integral-equation analysis (Kuvshinov *et al.* 1999b), finite-difference analysis (Uyeshima & Schultz 2000) and spectral finite-element analysis Martinec (1999). Progress has also been made in estimating frequency-domain responses from satellite data (Didwall 1984; Oraevsky *et al.* 1993; Olsen 1999). The methods commonly average out spatial geomagnetic variations. To better utilize the full information content of satellite induction data, and thus enhance resolution of conductivity variations in the Earth's mantle, a spatiotemporal analysis of geomagnetic induction is required.

*On leave from: Department of Geophysics, Faculty of Mathematics and Physics, Charles University, V Holešovičkách 2, 18000 Prague 8, Czech Republic.

In this paper, we will modify the existing frequency-domain 2-D hybrid spectral finite-element approach Martinec (1997) by the implementation of a time-stepping algorithm and model the transient geomagnetic response of a 2-D heterogeneous sphere directly in the time domain. The main purpose of this paper is to present the new time-domain, spectral finite-element approach in a transparent way. We will also validate the theory and associated numerical code by comparing the numerical results with a semi-analytical solution to 1-D and 2-D forward modelling of transient electromagnetic induction in a heterogeneous sphere consisting of a radially and axially symmetric configuration of nested spheres.

2 CLASSICAL AND WEAK FORMULATIONS OF THE ELECTROMAGNETIC INDUCTION PROBLEM

Our intention is to study the response of a conducting spherical Earth with an axisymmetric electrical conductivity distribution to an external electromagnetic excitation. This problem can be formulated mathematically as an initial, boundary-value problem for the magnetic diffusion equation. Martinec (1997) solved this problem in the Fourier-frequency domain using the spectral finite-element approach. In the following sections, we will modify this approach to compute the electromagnetic response in the time domain.

Let us assume that a conducting sphere G with electrical conductivity σ approximates a heterogeneous Earth. Let the surrounding region of G be a perfect insulator, representing the Earth's atmosphere in the near-space environment. The model G is excited by a specified source of external origin. The magnetic induction $\mathbf{B}_0$ outside the Earth (the subscript 0 denotes vacuum) is simply the negative gradient of the magnetic scalar potential U,

$$\mathbf{B}_0 = -\mathrm{grad}\, U \quad \text{outside } G, \tag{1}$$

where U satisfies the Laplace equation in the vacuum outside G. We assume that the external electromagnetic sources are axisymmetrically distributed. U is therefore an axisymmetric scalar and can be represented in terms of zonal scalar spherical harmonics $Y_j(\vartheta)$:

$$U(r,\vartheta,t) = a\sum_{j=1}^{\infty}\left[\left(\frac{r}{a}\right)^j G_j^{(e)}(t) + \left(\frac{a}{r}\right)^{j+1} G_j^{(i)}(t)\right] Y_j(\vartheta) \quad \text{for } r \geq a, \tag{2}$$

where r, ϑ and φ are spherical coordinates and $G_j^{(e)}(t)$ and $G_j^{(i)}(t)$ are the time-dependent, zonal spherical harmonic coefficients of the external electromagnetic sources and the magnetic field generated by the induced eddy currents in G, respectively. Note that the axisymmetric geometry allows us to abbreviate the notation and drop the azimuthal index $m = 0$ for spherical harmonics.

Using the gradient formula for spherical harmonics (Varshalovich *et al.* 1989), the magnetic induction in the vacuum ($r \geq a$) reads as

$$\mathbf{B}_0(r,\vartheta,t) = -\sum_{j=1}^{\infty}\left[\sqrt{j(2j+1)}\left(\frac{r}{a}\right)^{j-1} G_j^{(e)}(t)\mathbf{Y}_j^{j-1}(\vartheta) + \sqrt{(j+1)(2j+1)}\left(\frac{a}{r}\right)^{j+2} G_j^{(i)}(t)\mathbf{Y}_j^{j+1}(\vartheta)\right], \tag{3}$$

where $\mathbf{Y}_j^{j-1}(\vartheta)$ and $\mathbf{Y}_j^{j+1}(\vartheta)$ are the zonal spheroidal vector spherical harmonics. For the following considerations, it is convenient to express the magnetic induction $\mathbf{B}_0$ in terms of the toroidal vector potential $\mathbf{A}_0$ such that $\mathbf{B}_0 = \mathrm{rot}\, \mathbf{A}_0$. Using the rotation formulae for vector spherical harmonics Varshalovich *et al.* (1989), the spherical harmonic representation of the toroidal vector potential in a vacuum is

$$\mathbf{A}_0(r,\vartheta,t) = ia\sum_{j=1}^{\infty}\left[\sqrt{\frac{j}{j+1}}\left(\frac{r}{a}\right)^j G_j^{(e)}(t) - \sqrt{\frac{j+1}{j}}\left(\frac{a}{r}\right)^{j+1} G_j^{(i)}(t)\right]\mathbf{Y}_j^j(\vartheta), \tag{4}$$

where $i = \sqrt{-1}$ and $\mathbf{Y}_j^j(\vartheta)$ are the zonal toroidal vector spherical harmonics.

In this paper, we will confine ourselves to Earth models with an axially symmetric distribution of electrical conductivity, that is

$$\sigma = \sigma(r,\vartheta) \quad \text{in } G. \tag{5}$$

For the axisymmetric geometry of external sources and the conductivity model, it is advantageous to formulate the initial, boundary-value problem of the global-scale electromagnetic induction in the Earth in terms of the toroidal vector potential. The classical mathematical formulation is as follows. Find the toroidal vector potential $\mathbf{A} \in C^2(\overline{G}) \times C^1(\langle 0,\infty))$ such that $\mathbf{B} = \mathrm{rot}\, \mathbf{A}$ and

$$\frac{1}{\mu}\,\mathrm{rot}\,\mathrm{rot}\,\mathbf{A} + \sigma\frac{\partial \mathbf{A}}{\partial t} = \mathbf{0} \quad \text{in } G, \tag{6}$$

$$\mathrm{div}\,\mathbf{A} = 0 \quad \text{in } G, \tag{7}$$

$$\mathbf{n} \times \mathrm{rot}\,\mathbf{A} = \mathbf{b}_0 \quad \text{on } \partial G, \tag{8}$$

where the conductivity $\sigma \geq 0$ is a continuous function in G, $\sigma \in C(G)$, $\mu > 0$ is the constant permittivity of vacuum, and $\mathbf{b}_0(\vartheta,t) \in C^2(\partial G) \times C^1(\langle 0,\infty))$ is the tangential component of magnetic induction $\mathbf{B}$ on the external surface ∂G at time $t \geq 0$,

$$\mathbf{b}_0 := \mathbf{n} \times \mathbf{B}_0|_{\partial G}\,, \tag{9}$$

and $\mathbf{n}$ is the normal to ∂G. At the internal interfaces, where the electrical conductivity changes discontinuously, the continuity of the tangential components of magnetic induction end electric intensity are required (Weaver 1994 , eqs 1.82 and 1.83). The various function spaces are listed in Table 1.

Let us turn our attention to the weak (variational) formulation of the problem. We first introduce the solution space V as

$$V := \{\mathbf{f} \,|\, \mathbf{f} \in L_2(G),\ \mathrm{rot}\,\mathbf{f} \in L_2(G),\ \mathrm{div}\,\mathbf{f} = 0 \text{ in } G\}\,. \tag{10}$$

Following Martinec (1997), the weak formulation of the initial, boundary-value problem, eqs (6)–(8), consists of finding the potential $\mathbf{A} \in V \times C^1(\langle 0,\infty))$ such that at a fixed time it satisfies the following variational equality:

$$a(\mathbf{A},\delta\mathbf{A}) + b(\mathbf{A},\delta\mathbf{A}) = F(\delta\mathbf{A}) \quad \forall \delta\mathbf{A} \in V, \tag{11}$$

Table 1. List of function spaces used.

$C(\overline{G})$	Space of the continuous functions defined in G
$C^1(\langle 0,\infty))$	Space of the functions for which the classical derivatives up to first order are continuous on the interval $\langle 0,\infty)$
$C^2(\overline{G})$	Space of the functions for which the classical derivatives up to second order are continuous in the domain $\overline{G}$
$L_2(G)$	Space of square-integrable functions in the domain G

where the sesquilinear forms $a(\cdot\ ,\ \cdot)$, $b(\cdot\ ,\ \cdot)$ and the functional $F(\cdot)$ are defined as follows:

$$a(\mathbf{A}, \delta\mathbf{A}) := \frac{1}{\mu}\int_G (\mathrm{rot}\overline{\mathbf{A}} \cdot \mathrm{rot}\,\delta\mathbf{A})\, dV, \tag{12}$$

$$b(\mathbf{A}, \delta\mathbf{A}) := \int_G \sigma(r,\vartheta)\left(\frac{\partial\overline{\mathbf{A}}}{\partial t}\cdot\delta\mathbf{A}\right) dV, \tag{13}$$

$$F(\delta\mathbf{A}) := -\frac{1}{\mu}\int_{\partial G} (\overline{\mathbf{b}}_0 \cdot \delta\mathbf{A})\, dS, \tag{14}$$

and $\overline{\mathbf{A}} = \mathrm{Re}\,\mathbf{A} - i\,\mathrm{Im}\,\mathbf{A}$. We can see that the assumptions imposed on the potential $\mathbf{A}$ are weaker in the weak formulation than in the classical formulation. Moreover, the assumptions on the electrical conductivity σ and the boundary data $\mathbf{b}_0$ can also be made weaker in the latter formulation. It is sufficient to assume that the electrical conductivity is a square-integrable function in G, $\sigma \in L_2(G)$, and the boundary data at a fixed time is a square-integrable function on ∂G, $\mathbf{b}_0 \in L_2(\partial G) \times C^1(\langle 0, \infty)$.

3 SPHERICAL HARMONIC PARAMETRIZATION

For the axisymmetric geometry of external sources and the conductivity model, Martinec (1997) showed that the induced electromagnetic field is axisymmetric and the associated toroidal vector potential is an axisymmetric vector. It may be represented in terms of zonal toroidal vector spherical harmonics $\mathbf{Y}_j^j(\vartheta)$. Their explicit forms are as follows (Varshalovich *et al.* 1989):

$$\mathbf{Y}_j^j(\vartheta) := -i\,P_{j1}(\cos\vartheta)\mathbf{e}_\varphi, \tag{15}$$

where $P_{j1}(\cos\vartheta)$ is the associated Legendre function of degree j and order $m = 1$, and $\mathbf{e}_\varphi$ is the spherical base vector in the φ-direction. An important property of the functions $\mathbf{Y}_j^j(\vartheta)$ is that they are divergence-free:

$$\mathrm{div}\left[f(r)\mathbf{Y}_j^j(\vartheta)\right] = 0, \tag{16}$$

where $f(r)$ is a differentiable function.

The required toroidal vector potential $\mathbf{A}$ and test functions $\delta\mathbf{A}$ can be expressed in terms of the functions $\mathbf{Y}_j^j(\vartheta)$ as follows:

$$\left\{\begin{matrix}\mathbf{A}\\ \delta\mathbf{A}\end{matrix}\right\} = \sum_{j=1}^{\infty}\left\{\begin{matrix}A_j^j(r,t)\\ \delta A_j^j(r)\end{matrix}\right\}\mathbf{Y}_j^j(\vartheta), \tag{17}$$

where $A_j^j(r,t)$ and $\delta A_j^j(r)$ are spherical harmonic expansion coefficients. The divergence-free property of functions $\mathbf{Y}_j^j(\vartheta)$ implies that both the toroidal vector potential $\mathbf{A}$ and test functions $\delta\mathbf{A}$ are divergence-free. Therefore, the parametrization (17) of potentials $\mathbf{A}$ and $\delta\mathbf{A}$ automatically satisfies the requirement on the functions from the solution space V to be divergence-free.

Spherical harmonic parametrizations of the sesquilinear forms $a(\cdot\ ,\ \cdot)$, $b(\cdot\ ,\ \cdot)$ and the functional $F(\cdot)$ are Martinec (1997)

$$a(\mathbf{A}, \delta\mathbf{A}) = \frac{1}{\mu}\sum_{j=1}^{\infty}\sum_{\ell=j-1}^{j+1,2}\int_0^a R_j^\ell(\overline{\mathbf{A}};r)R_j^\ell(\delta\mathbf{A};r)r^2\, dr, \tag{18}$$

$$b(\mathbf{A}, \delta\mathbf{A}) = \int_0^a \mathcal{E}(\mathbf{A}, \delta\mathbf{A};r)r^2\, dr, \tag{19}$$

$$F(\delta\mathbf{A}) = -\frac{ia^2}{\mu}\sum_{j=1}^{\infty}\sqrt{j(j+1)}\left[G_j^{(e)}(t) + G_j^{(i)}(t)\right]\delta A_j^j(a), \tag{20}$$

where $R_j^\ell(\mathbf{A};r)$ are the radial parts of the rot of $\mathbf{A}$,

$$R_j^{j-1}(\mathbf{A};r) = i\sqrt{\frac{j+1}{2j+1}}\left(\frac{d}{dr} + \frac{j+1}{r}\right)A_j^j(r),$$

$$R_j^{j+1}(\mathbf{A};r) = i\sqrt{\frac{j}{2j+1}}\left(\frac{d}{dr} - \frac{j}{r}\right)A_j^j(r), \tag{21}$$

and $\mathcal{E}$ denotes the angular part of the ohmic energy,

$$\mathcal{E}(\mathbf{A}, \delta\mathbf{A};r) = 2\pi\int_0^\pi \sigma(r,\vartheta)\sum_{j_1=1}^{\infty}\frac{\partial\overline{A}_{j_1}^{j_1}(r,t)}{\partial t}P_{j_1,1}(\cos\vartheta) \times \sum_{j_2=1}^{\infty}\delta A_{j_2}^{j_2}(r)P_{j_2,1}(\cos\vartheta)\sin\vartheta\, d\vartheta. \tag{22}$$

4 TOROIDAL ELECTRIC INTENSITY

The solution of the electromagnetic initial, boundary-value problem must satisfy yet another boundary condition that the toroidal component of electric intensity must pass through the Earth's surface continuously,

$$\boldsymbol{E} = \boldsymbol{E}_0 \quad \text{on } \partial G, \tag{23}$$

where $\boldsymbol{E}$ and $\boldsymbol{E}_0$ are the toroidal electric intensities in model G and the vacuum, respectively. Because of the axially symmetric configuration of electrical conductivity and external sources, the toroidal electric intensity can be written as the negative time derivative of the toroidal vector potential, $\boldsymbol{E} = -\partial\mathbf{A}/\partial t$. In view of this, the boundary condition (23) can alternatively be expressed in the form

$$\mathbf{A} = \mathbf{A}_0 \quad \text{on } \partial G. \tag{24}$$

Substituting for the spherical harmonics representation of $\mathbf{A}$ from eq. (17) and for $\mathbf{A}_0$ from eq. (4) results in the formula for unknown coefficients $G_j^{(i)}(t)$, which are expressed in terms of the prescribed spherical harmonics $G_j^{(e)}(t)$ of external sources and the coefficients $A_j^j(a,t)$ of the required solution:

$$G_j^{(i)}(t) = \frac{j}{j+1}G_j^{(e)}(t) + \frac{i}{a}\sqrt{\frac{j}{j+1}}A_j^j(a,t). \tag{25}$$

The last relation enables us to eliminate the unknown coefficients $G_j^{(i)}(t)$ from the system of eqs (11). The modified system has the form

$$a_1(\mathbf{A}, \delta\mathbf{A}) + b(\mathbf{A}, \delta\mathbf{A}) = F_1(\delta\mathbf{A}) \quad \forall\delta\mathbf{A} \in V, \tag{26}$$

where the new sesquilinear form $a_1(\cdot\ ,\ \cdot)$ and the new functional $F_1(\cdot)$ are expressed in terms of the original quantities and the coefficient $A_j^j(a,t)$ as follows:

$$a_1(\mathbf{A}, \delta\mathbf{A}) = a(\mathbf{A}, \delta\mathbf{A}) + \frac{a}{\mu}\sum_{j=1}^{\infty} j\overline{A}_j^j(a,t)\delta A_j^j(a), \tag{27}$$

$$F_1(\delta\mathbf{A}) = -\frac{ia^2}{\mu}\sum_{j=1}^{\infty}\sqrt{\frac{j}{j+1}}(2j+1)G_j^{(e)}(t)\delta A_j^j(a). \tag{28}$$

There is a difference in principle between the original eq. (11) and the modification (26) in prescribing the boundary data on the external surface ∂G. Eq. (11) requires the prescription of the horizontal

components of the total magnetic induction in a vacuum on ∂G. Inspecting the functional $F(\cdot)$ in eq. (20) shows that this requirement leads to the necessity to define linear combinations $G_j^{(e)}(t) + G_j^{(i)}(t)$, $j = 1, 2, \ldots$, as input boundary data for solving eq. (11). In contrast to this scheme, the functional $F_1(\cdot)$ on the right-hand side of eq. (26) only contains the spherical harmonic coefficients $G_j^{(e)}(t)$, see eq. (28). Hence, to solve eq. (26), only the spherical harmonic coefficients $G_j^{(e)}(t)$ of the external electromagnetic source are to be prescribed while the spherical harmonic coefficients $G_j^{(i)}(t)$ of the induced magnetic field within the Earth are determined after solving eq. (26) by means of relation (25). The former scheme is advantageous in the case where there is no possibility of separating the external and internal parts of surface magnetic induction observations by spherical harmonic analysis. The latter scheme can be applied if such an analysis can be carried out or in the case when the external magnetic source is defined by a known physical process.

5 FINITE-ELEMENT APPROXIMATION OVER THE RADIAL COORDINATE

We divide the range of integration $\langle 0, a\rangle$ into P subintervals by the nodes $0 = r_1 < r_2 < \cdots < r_P < r_{P+1} = a$. The piecewise linear basis functions defined by the relation $\psi_k(r_i) = \delta_{ki}$ can be used as the basis function of the Sobolev functional space $W_2^1(0, a)$. Note that only two basis functions are non-zero on the interval $r_k \le r \le r_{k+1}$, namely

$$\psi_k(r) = \frac{r_{k+1} - r}{h_k}, \quad \psi_{k+1}(r) = \frac{r - r_k}{h_k}, \tag{29}$$

where $h_k = r_{k+1} - r_k$. Since both the unknown solution $A_j^j(r, t)$ and test functions $\delta A_j^j(r)$ are elements of this functional space, they can be approximated by piecewise linear finite elements $\psi_k(r)$,

$$\begin{Bmatrix} A_j^j(r,t) \\ \delta A_j^j(r) \end{Bmatrix} = \sum_{k=1}^{P+1} \begin{Bmatrix} A_j^{j,k}(t) \\ \delta A_j^{j,k} \end{Bmatrix} \psi_k(r). \tag{30}$$

6 FREQUENCY-DOMAIN AND TIME-DOMAIN SOLUTIONS

We now present two approaches to solving the initial, boundary-value problem of electromagnetic induction with respect to the time variable t.

We first solve the variational equality (26) in the Fourier-frequency domain assuming that all field variables have a harmonic time dependence of the form $\mathrm{e}^{i\omega t}$.[1] Denoting the Fourier image of $\mathbf{A}$ by $\hat{\mathbf{A}}$, the weak formulation of electromagnetic induction in the frequency domain is described by the equation

$$a_1(\hat{\mathbf{A}}, \delta\hat{\mathbf{A}}) + i\omega b_1(\hat{\mathbf{A}}, \delta\hat{\mathbf{A}}) = F_1(\delta\hat{\mathbf{A}}) \quad \forall \delta\hat{\mathbf{A}} \in V, \tag{31}$$

where the sesquilinear form $b_1(\hat{\mathbf{A}}, \delta\hat{\mathbf{A}})$ is defined by

$$b_1(\hat{\mathbf{A}}, \delta\hat{\mathbf{A}}) := \int_G \sigma(r, \vartheta)(\overline{\hat{\mathbf{A}}} \cdot \delta\hat{\mathbf{A}})\, dV. \tag{32}$$

Having solved eq. (31) for $\hat{\mathbf{A}}$, the solution is transformed back to the time domain by applying the inverse Fourier transform.

Alternatively, the initial, boundary-value problem can be solved directly in the time domain. We have several choices for representing the time derivative of the toroidal vector potential $\mathbf{A}$ in the sesquilinear form $b(\cdot\,,\cdot)$. For simplicity, we will choose the explicit Euler differencing scheme Press *et al.* (1992):

$$\frac{\partial \mathbf{A}}{\partial t} \approx \frac{\mathbf{A}(r, \vartheta, t_{i+1}) - \mathbf{A}(r, \vartheta, t_i)}{t_{i+1} - t_i} =: \frac{{}^{i+1}\mathbf{A} - {}^{i}\mathbf{A}}{\Delta t_i}, \tag{33}$$

where ${}^{i}\mathbf{A}$ denotes the values of $\mathbf{A}$ at discrete time levels $t_0 < t_1 < \cdots < t_{i+1} < \cdots$. Eq. (26), which is now solved at each time level t_i, $i = 0, 1, \ldots$, has the form

$$a_1({}^{i+1}\mathbf{A}, \delta\mathbf{A}) + \frac{1}{\Delta t_i} b_1({}^{i+1}\mathbf{A}, \delta\mathbf{A}) = \frac{1}{\Delta t_i} b_1({}^{i}\mathbf{A}, \delta\mathbf{A}) + F_1\left({}^{i+1}G_j^{(e)}, \delta\mathbf{A}\right) \quad \forall \delta\mathbf{A} \in V, \tag{34}$$

where the sesquilinear form $b_1(\cdot\,,\cdot)$ is defined by eq. (32).

7 SPECTRAL FINITE-ELEMENT SOLUTION

Finally, we are ready to introduce the spectral finite-element solution to the initial, boundary-value problem of electromagnetic induction. We construct the functional space

$$V_h = \left\{ \delta\mathbf{A} = \sum_{j=1}^{j_{\max}} \sum_{k=1}^{P+1} \delta A_j^{j,k} \psi_k(r) \mathbf{Y}_j^j(\vartheta) \right\}, \tag{35}$$

where $j_{\max}$ and P are finite cut-off degrees. The Galerkin method for approximating the solution to the problem (31) in the frequency domain consists in finding $\hat{\mathbf{A}}_h \in V_h$ such that

$$a_1(\hat{\mathbf{A}}_h, \delta\hat{\mathbf{A}}_h) + i\omega b_1(\hat{\mathbf{A}}_h, \delta\hat{\mathbf{A}}_h) = F_1(\delta\hat{\mathbf{A}}_h) \quad \forall \delta\hat{\mathbf{A}}_h \in V_h. \tag{36}$$

The discrete solution $\hat{\mathbf{A}}_h$ of the Galerkin system of linear algebraic equations will be called the *frequency-domain, spectral finite-element solution*.

Likewise, the solution to the problem (34) in the time domain at a fixed time t_{i+1} is approximated by ${}^{i+1}\mathbf{A}_h \in V_h$ satisfying the equation

$$a_1\left({}^{i+1}\mathbf{A}_h, \delta\mathbf{A}_h\right) + \frac{1}{\Delta t_i} b_1\left({}^{i+1}\mathbf{A}_h, \delta\mathbf{A}_h\right) = \frac{1}{\Delta t_i} b_1\left({}^{i}\mathbf{A}_h, \delta\mathbf{A}_h\right) + F_1\left({}^{i+1}G_j^{(e)}, \delta\mathbf{A}_h\right) \quad \forall \delta\mathbf{A}_h \in V_h. \tag{37}$$

The discrete solution ${}^{i+1}\mathbf{A}_h$ of this system of equations is called the *time-domain, spectral finite-element solution*.

Inspecting eqs (36) and (37) from a numerical point of view, we can make the following remark. For a desired frequency ω and time t_{i+1}, the computation times required to set up the matrices of the system of equations (36) and (37) are the same. Moreover, the computation time for calculating the sesquilinear form $b_1(\cdot\,,\cdot)$ on the right-hand side of eq. (37) is significantly shorter than the time needed for solving this system of equations. Hence, the computation time required for solving eq. (36) for a frequency ω is slightly shorter, but comparable to the time needed for solving eq. (37) at time t_{i+1}.

8 VALIDATION

Before modelling the electromagnetic induction response of the Earth with a realistic conductivity structure, we will, as a first step, verify the time-domain, spectral finite-element approach against other solutions to the forward problem of global-scale electromagnetic induction in a heterogeneous spherical Earth. We therefore compare our results with analytical and semi-analytical solutions based on different methods of solution.

[1] The corresponding Fourier-transform equations are
$f(t) = \int_{-\infty}^{\infty} F(\omega)\mathrm{e}^{i\omega t} d\omega, \quad F(\omega) = \frac{1}{2\pi}\int_{-\infty}^{\infty} f(t)\mathrm{e}^{-i\omega t} dt.$

8.1 A mathematical model of external sources of a magnetic storm

We consider that the global-scale electromagnetic induction process in the Earth is induced by an external magnetic storm. We first introduce a simple mathematical model of its spatial and temporal structure.

During large geomagnetic storms, charged particles in the near-Earth plasma sheet are energized and injected deeper into the magnetosphere, producing the storm-time ring current. At mid-latitudes on the Earth's surface the magnetic potential due to this magnetospheric current has a nearly axisymmetric structure. It changes with colatitude predominantly as the cosine of the colatitude, that is, as the Legendre function $P_{10}(\cos\vartheta)$ (Eckhardt *et al.* 1963; Banks & Ainsworth 1992). The time development of a magnetic storm also follows a characteristic pattern. Its initial phase is characterized by a fast intensification of the ring current with a timescale of several hours. The following main phase of a storm, which can last as long as 2–2.5 d in the case of severe storms, is characterized by the occurrence of multiple intense substorms, with the associated auroral and geomagnetic effects. The final recovery phase of a storm is characterized by an exponential relaxation of the ring current to its usual intensity with a characteristic timescale of several days (Hultqvist 1973).

The complex structure of a magnetic storm will be described by a simple mathematical model that characterizes the basic features of a storm. The storm ring current is considered to be axisymmetric with a $P_{10}(\cos\vartheta)$ spatial structure. Consequently, all spherical harmonics of the external scalar magnetic potential are equal to zero except for the first-degree coefficient $G_j^{(e)}(t)$. After the onset of a magnetic storm at $t = 0$, the ring current quickly peaks and then decays exponentially. This time evolution is described by the function

$$G_1^{(e)}(t) = \sqrt{\frac{4\pi}{3}}\, A t \mathrm{e}^{-t/\tau}, \tag{38}$$

where $\sqrt{4\pi/3}$ is the inverse norm of $P_{10}(\cos\vartheta)$, A is the amplitude and τ is the relaxation time describing the recovery phase of a magnetic storm. Values typical of a moderate to large geomagnetic storm range from $\tau = 1$ day to 1 week (McPherron 1995). The Fourier image of $G_1^{(e)}(t)$ has an analytical form given by (Ben-Menahem & Singh 1981)

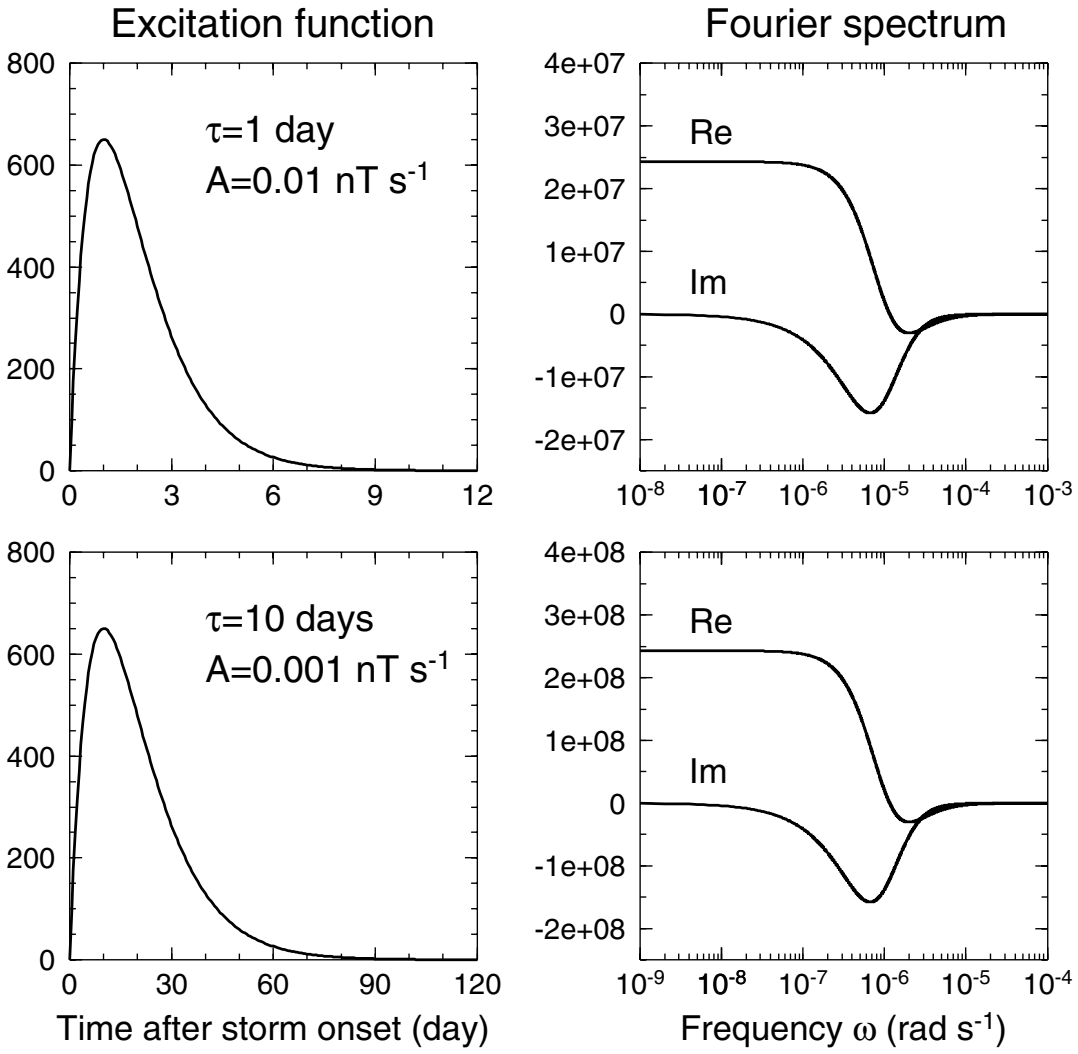

Figure 1. Transient ring-current excitation function $G_1^{(e)}(t)$ (in nT) with ring-current decay constant $\tau = 1$ d (amplitude $A = 0.01$ nT s^{-1}) and $\tau = 10$ d ($A = 0.001$ nT s^{-1}), respectively, and their Fourier spectra $G_1^{(e)}(\omega)$ (in nT s).

$$G_1^{(e)}(\omega) = \sqrt{\frac{4\pi}{3}}\frac{A}{2\pi}\frac{\alpha^2 - \omega^2 - 2i\alpha\omega}{(\alpha^2+\omega^2)^2}, \tag{39}$$

where ω is the angular frequency and $\alpha = 1/\tau$.

Scaling the relaxation time τ by a factor of k, it can be shown that the functions (38) and (39) satisfy the following properties:

$$G_1^{(e)}\left(\frac{t}{k}; kA, \frac{\tau}{k}\right) = G_1^{(e)}(t; A, \tau),$$
$$G_1^{(e)}\left(k\omega; k^2A, \frac{\tau}{k}\right) = G_1^{(e)}(\omega; A, \tau). \tag{40}$$

The scaling property in the time domain tells us that, scaling the t-axis by a factor of k, two excitation functions of the form (38) with relaxation times that differ by the factor k equal to each other if the amplitudes of these functions are scaled by a factor of k. The scaling property in the frequency domain can be interpreted analogously. Fig. 1 shows the excitation function (38) and its Fourier image (39) for two relaxation times, $\tau = 1$ d ($A = 0.01$ nT s^{-1}) and $\tau = 10$ d ($A = 0.001$ nT s^{-1}). The scaling property (40) is clearly demonstrated. If not specified otherwise, we will use $\tau = 10$ d and $A = 0.001$ nT s^{-1} in the following test examples.

8.2 Homogeneous and two-layer spheres

The time-domain, spectral finite-element solution is first checked by comparing it with analytical solutions for electromagnetic induction in a homogeneous sphere and in a two-layer sphere. The relevant analytical solution for the φ-component of the toroidal vector potential in the frequency domain is

$$A_\varphi(r, \vartheta, \omega) = -\frac{3}{2k}\frac{j_1(kr)}{j_0(ka)}\sin\vartheta\sqrt{\frac{3}{4\pi}}G_1^{(e)}(\omega) \tag{41}$$

for a homogeneous sphere with radius a and conductivity σ, where $k^2 = -i\omega\mu\sigma$. For a two-layer sphere, the solution is

$$A_\varphi(r, \vartheta, \omega) = -\frac{3}{2k_1}\frac{j_1(k_1r) + \Lambda(k_1, k_2, b)y_1(k_1r)}{j_0(k_1a) + \Lambda(k_1, k_2, b)y_0(k_1a)}\sin\vartheta\sqrt{\frac{3}{4\pi}}G_1^{(e)}(\omega), \tag{42}$$

where the inner sphere has radius b and conductivity σ_2 and the outer sphere radius a and conductivity σ_1. Eq. (42) is valid in the outer sphere, that is for radial distances $b \le r \le a$. We do not present an analytical formula for the potential A_φ in the inner sphere. In eqs (41) and (42), $j_j(kr)$ and $y_j(kr)$ are the spherical Bessel functions of the first and second kind, respectively Abramowitz & Stegun (1965), while $\Lambda(k_1, k_2, b)$ is the reflection coefficient:

$$\Lambda(k_1, k_2, b) := -\frac{k_1 j_0(k_1b)j_1(k_2b) - k_2 j_1(k_1b)j_0(k_2b)}{k_1 y_0(k_1b)j_1(k_2b) - k_2 y_1(k_1b)j_0(k_2b)}, \tag{43}$$

with $k_i^2 = -i\omega\mu\sigma_i$, $i = 1, 2$. The corresponding r- and ϑ-components of the magnetic induction **B** in the frequency domain are

$$B_r(r, \vartheta, \omega) = -\frac{3}{kr}\frac{j_1(kr)}{j_0(ka)}\cos\vartheta\sqrt{\frac{3}{4\pi}}G_1^{(e)}(\omega),$$
$$B_\vartheta(r, \vartheta, \omega) = \frac{3}{2kr}\frac{krj_0(kr) - j_1(kr)}{j_0(ka)}\sin\vartheta\sqrt{\frac{3}{4\pi}}G_1^{(e)}(\omega) \tag{44}$$

for a homogeneous sphere, and

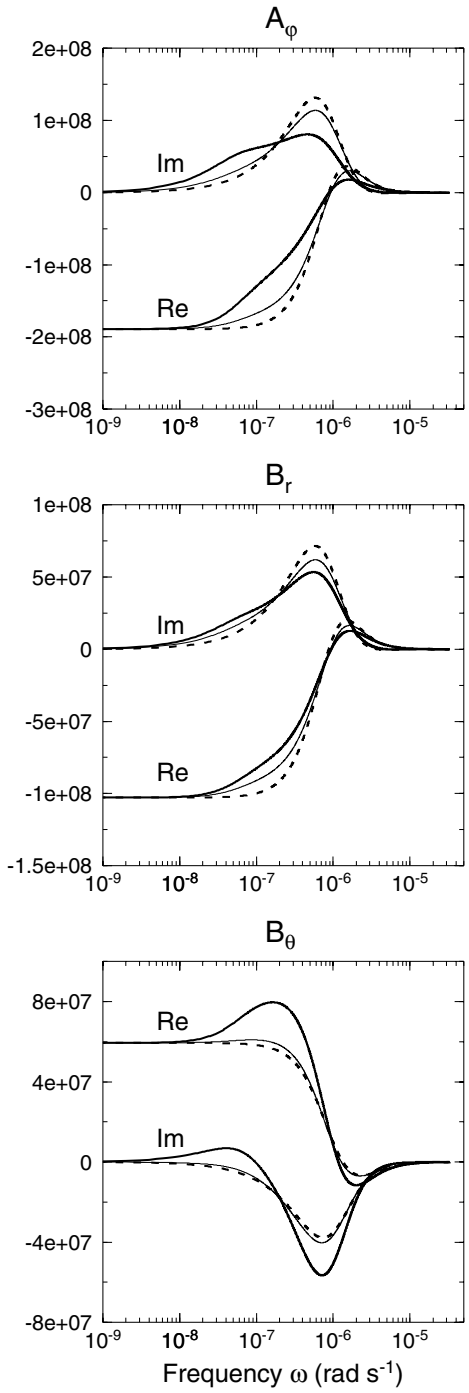

Figure 2. The real and imaginary parts of the surface magnetic-induction storm responses $A_\varphi(a, \vartheta, \omega)$ (in nT m s), $B_r(a, \vartheta, \omega)$ and $B_\vartheta(a, \vartheta, \omega)$ (in nT s) of a sphere to ring current excitation. Three sphere configurations are considered: (a) a homogeneous sphere with radius $a = 6371$ km and electrical conductivity $\sigma = 0.1$ S m^{-1} (dashed lines), (b) a two-layer sphere, in which the inner sphere has a radius $b = 3500$ km and conductivity $\sigma_2 = 10$ s m^{-1} and the outer sphere radius $a = 6371$ km and conductivity $\sigma_1 = 0.1$ s m^{-1} (thin solid lines) and (c) eccentrically nested spheres having the same geometrical and physical parameters as for the two-layer sphere, but with the inner sphere now translated along the z-axis by $d = 2700$ km (thick solid lines). Results apply to the colatitude $\vartheta = 30^\circ$. In all figures, A_φ is normalized by a real constant factor of 10^6 to simplify the plotting.

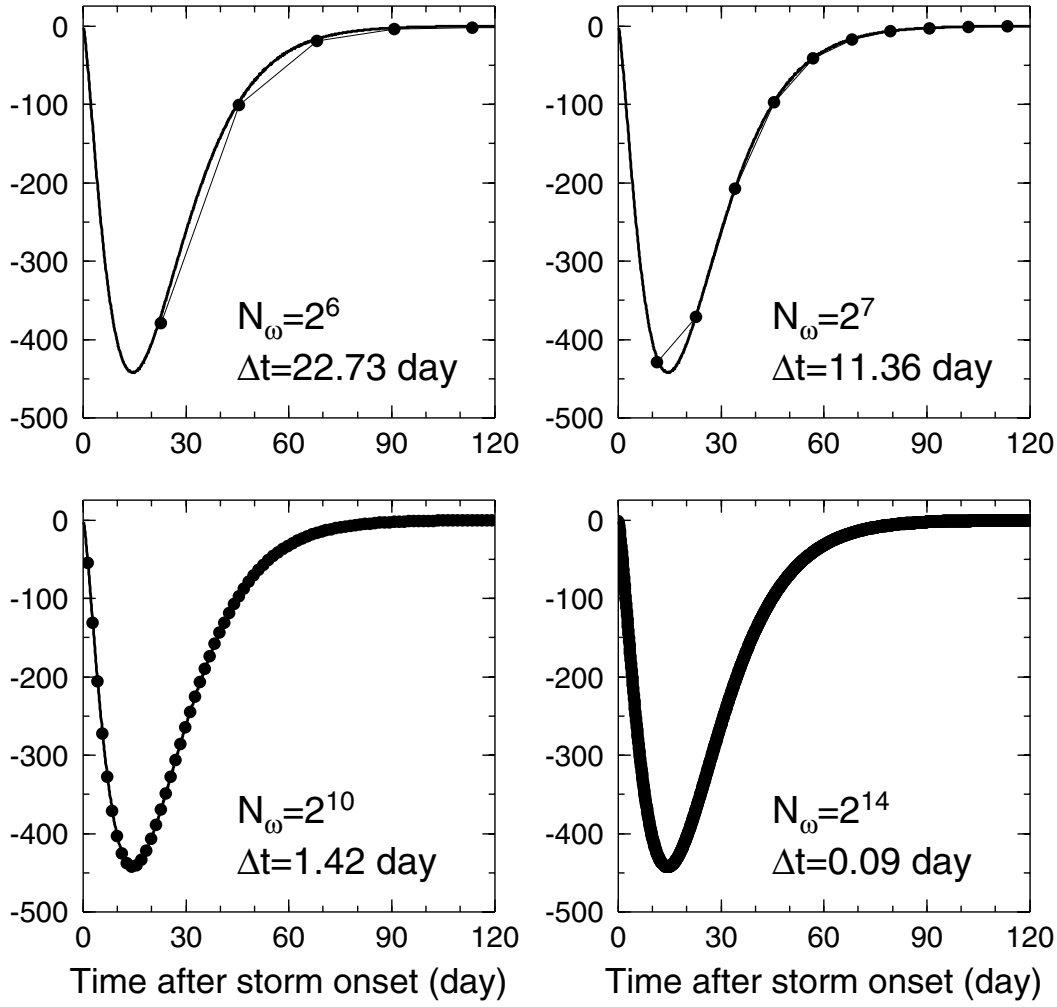

Figure 3. The surface magnetic-induction storm response function $A_\varphi(a, \vartheta, t)$ (in nT m) at the colatitude $\vartheta = 30^\circ$ as a function of time after the onset of a magnetic storm (38) for four different numbers of spectral samples, $N_\omega = 2^M$ (dots connected by a thin line). The responses $A_\varphi(a, \vartheta, t)$ are computed by the inverse fast Fourier transform of the analytical solution (41) with a fixed frequency step $\Delta\omega = 5 \times 10^{-8}$ rad s^{-1}. The corresponding time step is calculated according to relation $\Delta t = 2\pi/N_\omega\Delta\omega$. The inverse Fourier transform of the frequency-domain solution is compared with the time-domain solution (37) for the cut-off degree $j_{\max} = 1$, the number of finite elements $P = 60$, and time step $\Delta t = 0.09$ d (thick lines). The results apply to a homogeneous sphere of radius $a = 6371$ km and conductivity $\sigma = 0.1$ s m^{-1}.

$$B_r(r, \vartheta, \omega) = -\frac{3}{k_1 r}\frac{j_1(k_1 r) + \Lambda(k_1, k_2, b) y_1(k_1 r)}{j_0(k_1 a) + \Lambda(k_1, k_2, b) y_0(k_1 a)} \cos\vartheta \sqrt{\frac{3}{4\pi}} G_1^{(e)}(\omega),$$

$$B_\vartheta(r, \vartheta, \omega) = \frac{3}{2k_1 r} \times \frac{k_1 r j_0(k_1 r) - j_1(k_1 r) + \Lambda(k_1, k_2, b)[k_1 r y_0(k_1 r) - y_1(k_1 r)]}{j_0(k_1 a) + \Lambda(k_1, k_2, b) y_0(k_1 a)} \times \sin\vartheta \sqrt{\frac{3}{4\pi}} G_1^{(e)}(\omega) \quad (45)$$

for a two-layer sphere ($b \le r \le a$). Fig. 2 shows the real and imaginary parts of the φ-component of the surface toroidal vector magnetic potential and the r- and ϑ-components of the surface magnetic induction at colatitude $\vartheta = 30^\circ$ as a function of angular frequency ω for a homogeneous sphere (dashed lines) and a two-layer sphere (thin solid lines).

The analytical solutions (41)–(45) in the frequency domain are then transformed to time-domain solutions by applying the inverse Fourier transform. Since the solutions in the time domain are represented by real and causal functions, the inverse Fourier transform reduces to the cosine transform.[2] To implement this transform numerically, the limits of the Fourier images for $\omega \to 0$ need to be specified. Taking into account the limits of the spherical Bessel functions for the case when the argument approaches zero (Abramowitz & Stegun 1965), we find that

$$\lim_{\omega\to 0} \begin{Bmatrix} A_\varphi(r, \vartheta, \omega) \\ B_r(r, \vartheta, \omega) \\ B_\vartheta(r, \vartheta, \omega) \end{Bmatrix} = \begin{Bmatrix} -\frac{1}{2} r \sin\vartheta \\ -\cos\vartheta \\ \sin\vartheta \end{Bmatrix} \frac{A}{2\pi\alpha^2} \quad (46)$$

for both a homogeneous and a two-layer sphere model.

We now consider the transient electromagnetic-induction response of a homogeneous sphere of radius $a = 6371$ km and conductivity $\sigma = 0.1$ S m^{-1} to the ring-current excitation (38) with relaxation time $\tau = 10$ d and amplitude $A = 0.001$ nT s^{-1}. The inverse Fourier transform of the frequency-domain solution (41) is

[2]The corresponding cosine transform is $f(t) = 4\int_0^\infty \mathrm{Re}F(\omega)\cos\omega t\, d\omega$.

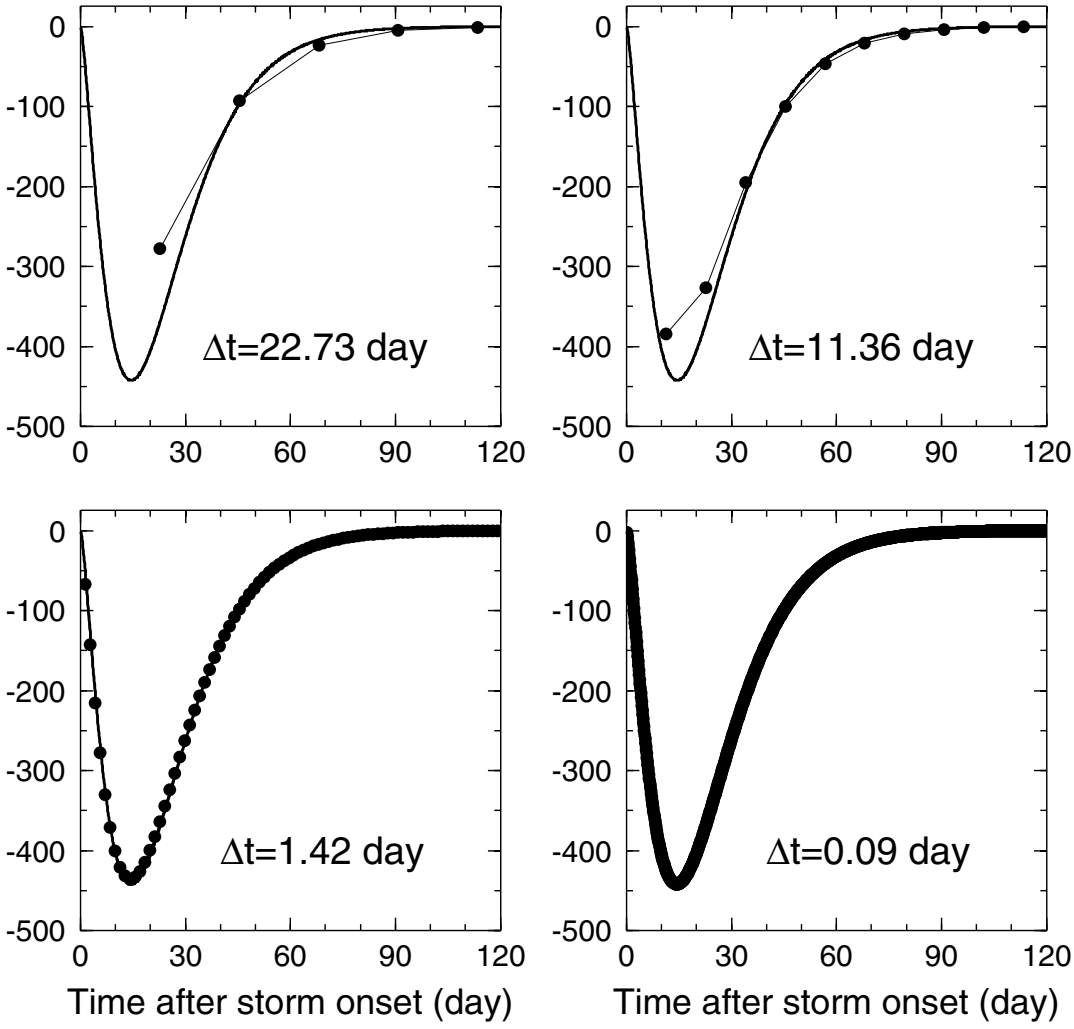

Figure 4. As in Fig. 3 but the response function $A_\varphi(a, \vartheta, t)$ is computed by the time-domain approach (37) for four different time steps (dots connected by a thin line). The thick lines correspond to the frequency-domain solution with the frequency step $\Delta\omega = 5 \times 10^{-8}$ rad s^{-1} and with the number of spectral samples $N_\omega = 2^{14}$.

computed numerically using the fast Fourier transform. For this calculation, the frequency step $\Delta\omega$ and the number of spectral samples $N_\omega = 2^M$ must be chosen. Inspecting Figs 1 and 2, we choose $\Delta\omega = 5 \times 10^{-8}$ rad s^{-1} and plot the inverse fast Fourier transform of $A_\varphi(\cdot\,, \cdot, \omega)$ for various N_ω (see Fig. 3). As expected, the time resolution of the resulting $A_\varphi(\cdot, \cdot, t)$ increases with increasing number of spectral samples N_ω because of $\Delta t = 2\pi/N_\omega\Delta\omega$. Comparing N_ω with the number of time steps, N_t, required to compute $A_\varphi(\cdot, \cdot, t)$ by the time-domain approach, $N_t = T/\Delta t + 1$, where T is a time interval of interest, we find that, in order to determine the response function $A_\varphi(\cdot, \cdot, t)$ with a particular resolution Δt by the frequency-domain approach, the corresponding function $A_\varphi(\cdot, \cdot, \omega)$ in the frequency domain must be evaluated at a larger number of frequencies than N_t. That is, in general, $N_\omega > N_t$ for transient electromagnetic excitations. For instance, the fourth panel in Fig. 3 shows that, in order to obtain a resolution of $\Delta t \approx 0.09$ d within the time interval $T =$ 0–120 d, the response function $A_\varphi(\cdot, \cdot, \omega)$ must be evaluated at $2^{14} =$ 16 384 frequencies, while the time-domain approach computes the response function $A_\varphi(\cdot, \cdot, t)$ in 1334 time instances. Moreover, the difference between N_ω and N_t increases if the frequency resolution $\Delta\omega$ becomes finer. In view of this and the remark made after eq. (37), we can say that the time-domain approach reduces the computation time required for determining a magnetic-induction response function to a transient excitation in comparison with the frequency-domain approach. Depending on the spectral properties of the transient excitation function, this reduction may be very significant. Note that the conclusion is opposite, that is $N_\omega < N_t$, or even $N_\omega \ll N_t$ for a monochromatic electromagnetic excitation.

The above conclusion is independent of the relaxation time τ of a magnetic storm (38) because of the relaxation-time scaling property (40). For instance, if the relaxation time τ is k-times shorter than in the previous example, the frequency step $\Delta\omega$ can be chosen to be k-times larger in the frequency-domain approach, while the number N_ω chosen is the same. In the time-domain approach, the time step Δt and the time interval T are chosen to be k times shorter, which implies that N_t is the same as above. For these choices, the relative resolutions in the frequency domain, $\Delta\omega/N_\omega\Delta\omega$, in the time domain, $\Delta t/T$, and the numbers N_ω and N_t are the same as in the previous example.

The approximation (33) of the time derivative is of first-order accuracy in time. We have investigated the size of the time step

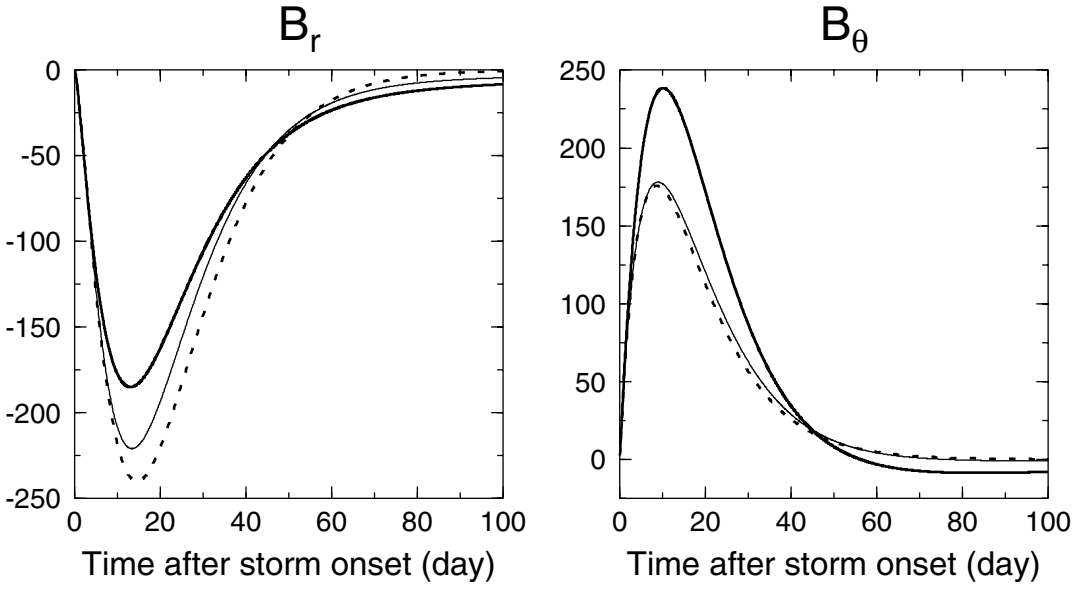

Figure 5. The surface transient magnetic responses $B_r(t)$ and $B_\vartheta(t)$ (in nT) of a homogeneous conductive sphere (dashed lines), the two-layer sphere (thin lines) and the eccentrically nested spheres (thick lines) at the colatitude $\vartheta = 30^\circ$ after the onset of a magnetic storm. The parameters of sphere configurations and of magnetic storm are the same as in Fig. 2.

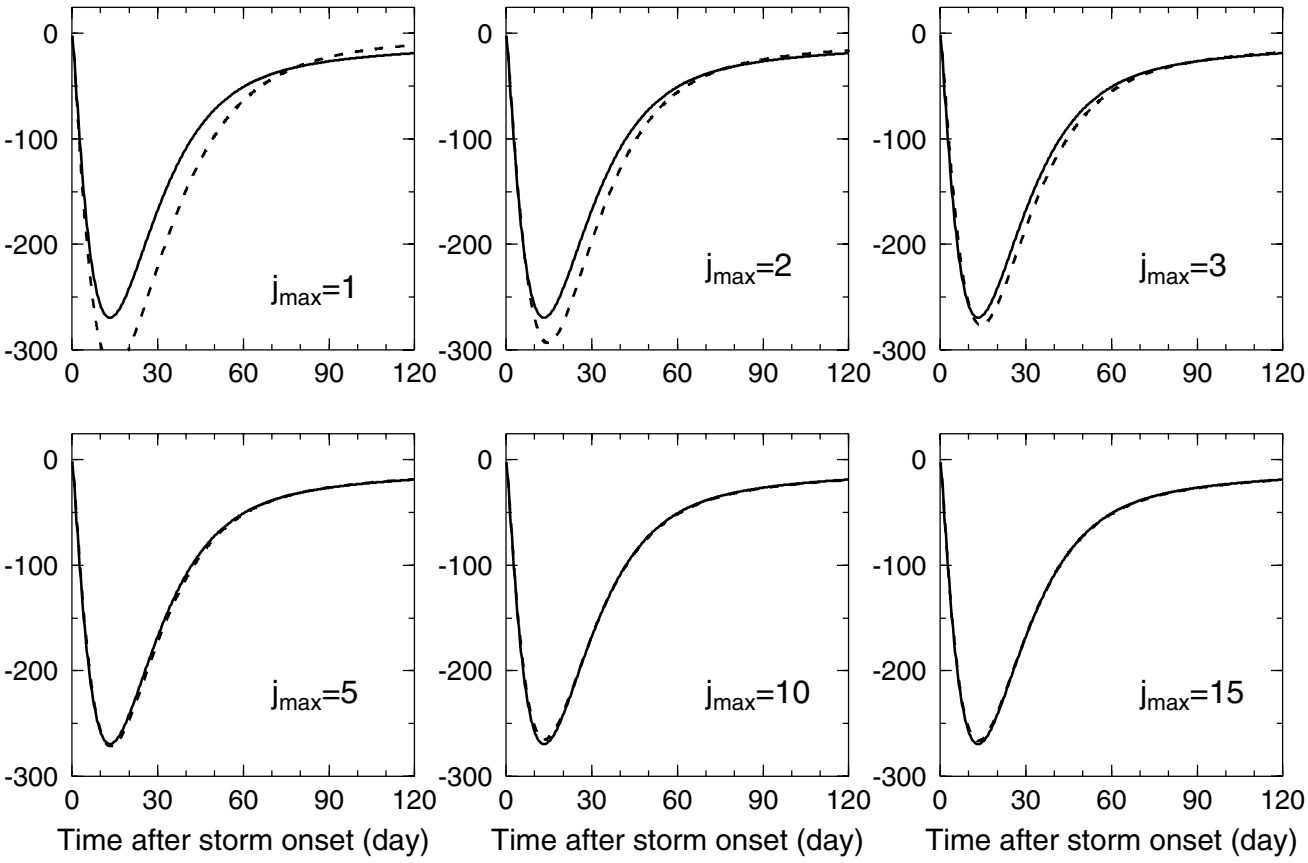

Figure 6. The convergence of the time-domain, spectral finite-element numerical solution (dashed lines) to the inverse Fourier transform of the semi-analytical, frequency-domain solution (solid lines) for the eccentrically nested spheres model. The surface magnetic-induction storm response function $A_\varphi(a, \vartheta, t)$ (in nT m) at the colatitude $\vartheta = 30^\circ$ as a function of time after the onset of a magnetic storm (38) is plotted for increasing value of the cut-off degrees $j_{\max}$. The number of finite elements in radial direction is fixed to $P = 60$. The parameters of the nested spheres configuration are the same as in Fig. 2.

needed to achieve a desired accuracy of the response functions in time. Fig. 4 shows the response function $A_\varphi(a, \vartheta, t)$ computed by the time-domain approach for four different time steps. We can see that $A_\varphi(a, \vartheta, t)$ converges to the response computed by the frequency-domain approach if the size of the time step is made finer. For instance, the relative difference between the two responses for $\Delta t =$ 0.09 d is less than 0.3 per cent.

The transient responses $B_r(t)$ and $B_\vartheta(t)$ of the homogeneous sphere, the two-layer sphere and the eccentrically nested spheres (we will deal with this configuration in the next section) at the external surface $r = a$ and for colatitude $\vartheta = 30^\circ$ are shown in Fig. 5 for the ring-current excitation described by eq. (38). The comparison of Figs 1 and 5 shows that the induced eddy currents persist for longer times after the storm onset than does the ring current. Fig. 5 also shows that the effect of the inner sphere in the two-layer sphere model on both the radial, $B_r(t)$, and the polar, $B_\vartheta(t)$, responses is small, because the frequency with the largest response corresponds to that which makes the skin depth roughly equal to the radius of the inner sphere. In contrast, the effect of the inner sphere in the eccentrically nested-sphere model is dominant, particularly at later times.

8.3 Eccentrically nested spheres model

The 2-D validation of the time-domain, spectral finite-element solution is based on a semi-analytical solution of electromagnetic induction in a sphere with an eccentrically nested spherical inclusion Everett & Schultz (1995). It is formulated in terms of the φ-component of the toroidal vector potential, which satisfies the scalar Helmholtz equation. This equation is valid for low-frequency magnetic fields inside source-free regions of the Earth with no spatial variation in the electrical conductivity. The magnetic induction in the inner and outer spheres, respectively, is expressed as truncated series of scalar spherical wavefunctions, the eigenfunctions of the scalar Helmholtz equation. The coefficients of the series expansions are determined from the continuity conditions of the tangential components of magnetic induction at the interface between the spheres, and the tangential and normal components of the magnetic induction at the Earth's surface. For further details, see Everett & Schultz (1995).

Fig. 2 (thick solid lines) shows the real and imaginary parts of the φ-component of the surface toroidal vector magnetic potential and the r- and ϑ-components of the surface magnetic induction at colatitude $\vartheta = 30^\circ$ as a function of angular frequency ω for the axially symmetric configuration of eccentrically nested spheres. The frequency-domain, semi-analytical response functions are then transformed to the time domain by the inverse Fourier transform and compared with the time-domain, spectral finite-element numerical response functions.

In Fig. 6, we change the cut-off degree $j_{\max}$ of the spherical harmonic expansion (35) of the toroidal vector potential **A** from $j_{\max} =$ 1 to $j_{\max} = 15$ (the number $P + 1$ of the finite elements in the radial direction is fixed, $P = 60$) and plot the time evolution of the φ-component of the surface toroidal vector potential **A** at colatitude $\vartheta = 30^\circ$ as a function of time after the onset of a magnetic storm of the form (38). The time-domain, spectral finite-element solutions (dashed lines) are checked by comparing them with the eccentrically nested-sphere solutions, computed semi-analytically

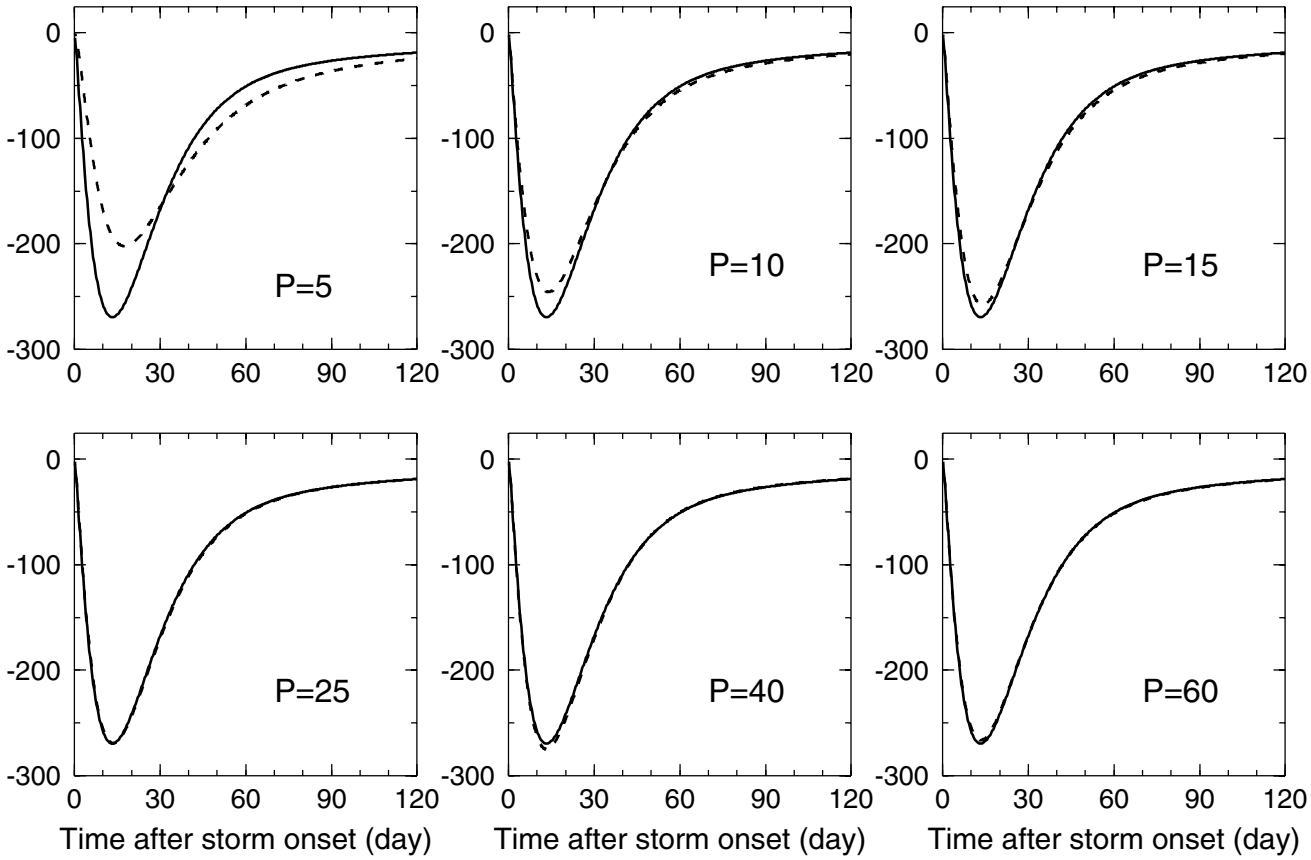

Figure 7. As Fig. 6. but for various numbers P of finite elements with the cut-off degree fixed to $j_{\max} = 15$.

in the frequency domain and inverted to the time domain by the inverse fast Fourier transform (solid lines). It is evident that the time-domain, spectral finite-element solution converges to the eccentrically nested-sphere solution as the cut-off degree $j_{\max}$ increases. For example, at $j_{\max} = 15$ (and $P = 60$), the relative difference between the two solutions is less than 1 per cent.

In Fig. 7, we illustrate a complementary test: we change the number $P + 1$ of linear finite elements in the radial direction and fix the cut-off degree $j_{\max}$ of the spherical harmonic expansion of the vector potential $\mathbf{A}$, $j_{\max} = 15$. We again observe that the time-domain, spectral finite-element solution quickly converges to the eccentrically nested-sphere solution as P increases.

9 CONCLUSION

The time-domain, spectral finite-element approach provides us with a powerful tool for the forward modelling of the electromagnetic-induction response of a spherical heterogeneous Earth to transient external current excitation. This approach is particularly appropriate when the spatial position of an observer is changing with time, such as the magnetometer on a satellite, or if the external source of electromagnetic induction has a complicated spatial and temporal distribution. In this paper, we have demonstrated this fact for a 2-D case when the electrical conductivity and external sources of electromagnetic variations are axisymmetrically distributed and when the external current excitation has a transient feature similar to that of a magnetic storm. The theory and numerical code, which have been tested by comparison with the analytical solution to electromagnetic induction within two concentrically nested spheres and with the Everett–Schultz semi-analytical solution to electromagnetic induction within two eccentrically nested spheres may serve as a means of validating 3-D spherical-geometry forward modelling codes, e.g. the finite-element method (Everett & Schultz 1996) and the finite-difference method (Uyeshima & Schultz 2000).

By extending the present approach, the transient electromagnetic induction in a 3-D heterogeneous sphere will become possible to model. The major advantage of the axisymmetric configuration, the fact that the vector potential $\mathbf{A}$ reduces to a scalar quantity A_φ, no longer exists for a 3-D geometry. The vector potential is no longer unidirectional and, therefore, it must be represented not only by zonal but also tesseral and sectoral spherical vector harmonics. However, there are no major difficulties in implementing a time-stepping method in the existing 3-D hybrid spectral finite-element method (Martinec 1999) or in the fully 3-D finite-element method (Everett & Schultz 1996). Work on these implementations is now in progress.

ACKNOWLEDGMENTS

We thank Detlef Wolf and two anonymous reviewers for their comments on the manuscript. This paper is a contribution to the SEAL (Sea Level Change) project, German Federal Ministry of Education and Research (BMBF) Project no SF2000/13. The research presented in this paper was partly supported by the Grant Agency of the Czech Republic through Grant no 205/00/1367 and by the National Research Council COBASE (Collaboration in the Basic Sciences and Engineering) US–Central Europe scientific exchange programme.

REFERENCES

Abramowitz, M. & Stegun, I.A., 1965. *Handbook of Mathematical Functions,* Dover, New York.

Banks, R.J. & Ainsworth, J.N., 1992. Global induction and the spatial structure of mid-latitude geomagnetic variations, *Geophys. J. Int.,* **110,** 251–266.

Ben-Menahem, A. & Singh, S.J., 1981. *Seismic Waves and Sources,* Springer-Verlag, New York.

Didwall, E.M., 1984. The electrical conductivity of the upper mantle as estimated from satellite magnetic field data, *J. geophys. Res.,* **89,** 537–542.

Eckhardt, D., Larner, K. & Madden, T., 1963. Long periodic magnetic fluctuations and mantle conductivity estimates, *J. geophys. Res.,* **68,** 6279–6286.

Everett, M.E. & Schultz, A., 1995. Geomagnetic induction in eccentrically nested spheres, *Phys. Earth planet. Inter.,* **92,** 189–198.

Everett, M.E. & Schultz, A., 1996. Geomagnetic induction in a heterogeneous sphere: azimuthally symmetric test computations and the response of an undulating 660-km discontinuity, *J. geophys. Res.,* **101,** 2765–2783.

Fainberg, E.B. & Singer, B.Sh., 1980. Electromagnetic induction in a non-uniform spherical model of the Earth, *Ann. Geophys.,* **36,** 127–134.

Hultqvist, B., 1973. Perturbations of the geomagnetic field, in *Cosmical Geophysics,* pp. 193–201, eds Egeland, A., Holter, O. & Omholt, A., Universitetsforlaget, Oslo.

Kuvshinov, A.V., Avdeev, D.B. & Pankratov, O.V., 1999a. Global induction by *Sq* and *Dst* sources in the presence of oceans: bimodal solutions for non-uniform spherical surface shells above radially symmetric Earth models in comparison to observations, *Geophys. J. Int.,* **137,** 630–650.

Kuvshinov, A.V., Avdeev, D.B., Pankratov, O.V. & Golyshev, S.A., 1999b. Modelling electromagnetic fields in 3-D spherical Earth using fast integral equation approach, *Expanded abstract of 2nd Int. Symp. on 3-D Electromagnetics,* 84–88.

McPherron, R.L., 1995. Magnetospheric dynamics, in *Introduction to Space Physics,* eds Kivelson, M.G. & Russell, C.T., Cambridge Univ. Press, Cambridge.

Martinec, Z., 1997. Spectral–finite element approach to two-dimensional electromagnetic induction in a spherical Earth, *Geophys. J. Int.,* **130,** 583–594.

Martinec, Z., 1999. Spectral–finite element approach to three-dimensional electromagnetic induction in a spherical Earth, *Geophys. J. Int.,* **136,** 229–250.

Neubert, T. *et al.*, 2001. Oersted satellite captures high-precision geomagnetic field data, *EOS, Trans. Am. geophys. Un.,* **82,** 81,87–88.

Olsen, N., 1999. Induction studies with satellite data, *Surv. Geophys.,* **20,** 309–340.

Oraevsky, V.N., Rotanova, N.M., Semenov, V.Yu, Bondar, T.N. & Abramova, D.Yu., 1993. Magnetovariational sounding of the Earth using observatory and MAGSAT satellite data, *Phys. Earth planet. Inter.,* **78,** 119–130.

Press, W.H., Teukolsky, S.A., Vetterling, W.T. & Flannery, B.P., 1992. *Numerical Recipes in Fortran. The Art of Scientific Computing,* Cambridge Univ. Press, Cambridge.

Uyeshima, M. & Schultz, A., 2000. Geoelectromagnetic induction in a heterogeneous sphere: a new three-dimensional forward solver using a conservative staggered-grid finite difference method, *Geophys. J. Int.,* **140,** 636–650.

Varshalovich, D.A., Moskalev, A.N. & Khersonskii, V.K., 1989. *Quantum Theory of Angular Momentum,* World Scientific, Singapore.

Weiss, C.J. & Everett, M.E., 1998. Geomagnetic induction in a heterogeneous sphere: fully three-dimensional test computations and the response of a realistic distribution of oceans and continents, *Geophys. J. Int.,* **135,** 650–662.

Weaver, J.T., 1994. *Mathematical Methods for Geo-electromagnetic Induction,* Research Studies Press, Wiley, New York.